

Synthesis and color properties of MnTiO₃ black ceramic pigment

Qikun Wang^{a,1,*}, Fanbing Lai^{a,1}, Wei Shi^{a,b}, Xiaohong Li^b, Renhua Chen^c, Huafeng Liu^c,
Xiaozhen Zhang^a, Qibing Chang^a, Yongqing Wang^{a,**}

^a School of Materials Science and Engineering, Jingdezhen Ceramic University, Jingdezhen, 333403, PR China

^b National Engineering Research Center for Domestic and Building Ceramics, Jingdezhen Ceramic University, Jingdezhen, 333000, PR China

^c Jiangxi Jinhuan Pigments Co., Ltd, Yichun, Jiangxi, 336000, PR China

ARTICLE INFO

Keywords:

MnTiO₃
Black pigment
Color properties
Tinting performance
Color mechanism

ABSTRACT

In this paper, MnTiO₃ powder has synthesized by solid-state method, and its color properties were also investigated. Research indicates that the L*-value of the prepared MnTiO₃ powder was only 25.85, showing a pure and deep black hue, which indicates that MnTiO₃ can be used as a black ceramic pigment and coating. The color mechanism of MnTiO₃ pigment is attributed to the ⁶A_{1g}→⁴A_{1g} and ⁶A_{1g}→⁴T_{2g} crystal field transition of octahedral Mn²⁺ site. Besides, the MnTiO₃ pigment exhibited outstanding tinting performance in ceramic glaze. The L*-v alue of the glaze sample with 8 wt% MnTiO₃ pigment added was only 11.44, which is the minimum value reported in the literature. Moreover, the MnTiO₃ pigmented coating shows an excellent solar energy utilization performance. This work demonstrates the promising application of MnTiO₃ pigment in ceramic decoration and solar absorber.

1. Introduction

In the ceramic decoration system (cyan-magenta-yellow-black system), black ceramic pigment is a crucial element, which has the dual roles: to act as a basic color and adjust the lightness of the pattern [1]. There are currently two main black ceramic pigments, i.e., zircon encapsulated carbon pigment (C@ZrSiO₄) and Co/Cr/Ni-containing metallic oxide-based pigments (e.g., CoFe₂O₄ and Cr-Fe₂O₃) [2–6]. Unfortunately, these two pigments have their drawbacks. Specially, lower encapsulation efficiency and a non-ideal lightness value (L* > 30) limit its widespread application of C@ZrSiO₄ black pigment [7–9]. Similarly, Co/Cr/Ni-containing metallic oxide-based black pigments have been criticized for expensive and a potential environmental threat [2,10,11]. More seriously, the color properties of the metallic oxide-based black pigments are sensitive to the chemical composition of the base glaze, so they are hard to provide a pure black hue to ceramic glaze [1,8]. In brief, it is significantly meaningful to develop a high color performance, cheap and environmentally friendly black ceramic pigment.

MnTiO₃ is one of the perovskite type materials, which has attracted attention for its excellent photocatalytic, magnetism, multiferoic, electrochemical properties, and so on [12–16]. Whereas, the color properties of MnTiO₃ seem to be overlooked. It has been reported that MnTiO₃ has strong light absorption in the visible region, indicating that it has the potential as a black pigment [17,18]. To date, no research to our knowledge has examined the color properties of MnTiO₃.

In this contribution, MnTiO₃ black pigment was synthesized via solid-state route. X-ray diffraction (XRD), thermogravimetric analysis/differential thermal analysis (TG/DTA), scanning electron microscopy (SEM), transmission electron microscopy (TEM), Selected area electron diffraction (SEAD), X-ray photoelectron spectroscopy (XPS), ultraviolet-visible spectroscopy (UV-vis) and other testing techniques were used to characterize the MnTiO₃ pigment and the corresponding glaze samples. The aim of the present work is to investigate the color properties and tinting performance of MnTiO₃ pigment. Moreover, the tinting mechanism of MnTiO₃ pigment in glaze was also discussed.

In this contribution, MnTiO₃ black pigment was synthesized via solid-state route. X-ray diffraction (XRD), thermogravimetric analysis/differential thermal analysis (TG/DTA), scanning electron microscopy (SEM), transmission electron microscopy (TEM), Selected area electron diffraction (SEAD), X-ray photoelectron spectroscopy (XPS), ultraviolet-visible spectroscopy (UV-vis) and other testing techniques were used to characterize the MnTiO₃ pigment and the corresponding glaze samples. The aim of the present work is to investigate the color properties and tinting performance of MnTiO₃ pigment. Moreover, the tinting mechanism of MnTiO₃ pigment in glaze was also discussed.

* Corresponding author.

** Corresponding author.

E-mail addresses: 19B309004@stu.hit.edu.cn (Q. Wang), 1436328003@qq.com (F. Lai), 034135@jci.edu.cn (W. Shi), lihong7178@163.com (X. Li), 35133293@qq.com (R. Chen), 1024965853@qq.com (H. Liu), zhangxz05@126.com (X. Zhang), changqibing@jci.edu.cn (Q. Chang), wyq8248@126.com (Y. Wang).

¹ Co-first authors, these authors contributed equally to this study and share co-first authorship.

<https://doi.org/10.1016/j.matchemphys.2023.127310>

Received 29 March 2022; Received in revised form 27 November 2022; Accepted 3 January 2023

0254-0584/© 20XX

2. Experiment procedure

2.1. Materials

Manganese monoxide (MnO, 99%), Titanium oxide (TiO₂, anatase, 99%) and Ethanol (CH₃CH₂OH, 99%) were purchased from Shanghai Titan Scientific Co., Ltd. Acrylic paint was obtained from Guangzhou Huakui Chemical Co., Ltd. All raw materials used without further purification.

2.2. Synthesis of MnTiO₃ black pigment

In a typical experiment for the preparation of MnTiO₃ pigment, 7.094 g of MnO, 7.980 g TiO₂ and 20.000 g of ethanol were mixed by mechanical grinding process in an agate mortar. The ethanol will volatilize during the mechanical grinding process. The precursor was obtained after the volatilization of ethanol. Finally, the precursor was calcinated at 1100 °C for 1 h to achieve the MnTiO₃ black pigment. In order to study the thermal evolution behavior of precursor, the precursor was also calcinated at 700 °C, 800 °C, 900 °C, 1000 °C, 1200 °C, respectively.

2.3. Application of MnTiO₃ pigment in ceramic glaze

To investigate the tinting performance of MnTiO₃ black pigment in a ceramic glaze, different amount (4 wt%, 6 wt%, 8 wt%, 10 wt%, 12 wt%) of MnTiO₃ pigment were added to base transparent glaze, respectively, and calcinated at 1200 °C for 20 min. Finally, the color glaze samples would be collected, and their performance would be tested. Table 1 lists the chemical compositions of the base transparent glaze.

2.4. Application of MnTiO₃ pigment in coating

To investigate the application of MnTiO₃ pigment in coatings, a MnTiO₃ pigmented coating was prepared. The fabrication process of the coating was as follows: firstly, MnTiO₃ paint was obtained by mechanical mixing 5 g of MnTiO₃ pigment and 5 g of acrylic paint in an agate mortar. And then, MnTiO₃ paint was evenly spread on a glass slide and left to dry at 80 °C for 12 h in an oven. Finally, the MnTiO₃ pigmented coating was obtained. For comparison, a control group and two coatings using commercial pigments were also prepared.

The solar energy utilization performance of MnTiO₃ pigmented coating was evaluated as follows: first, place the MnTiO₃ pigmented coating on an upside-down empty glass beaker to prevent heat conduction. An infrared lamp (Philips 250 W, 220 V) was used to simulate solar radiation. The distance between the coatings and the infrared lamp was maintained at 0.3 m. The temperature in laboratory maintaining at 30 °C (controlled by an air conditioner), and no wind. Finally, the temperature changes of the coatings within a 60 min periods were recorded with an infrared thermometer (AS842B, SMART SENSOR).

2.5. Characterization

A series of test techniques were used to characterize the MnTiO₃ black pigments and the color glaze samples. Phase compositions of the pigments and the glaze samples were analyzed by X-ray diffraction analysis (XRD, Bruker D8 Advance X-ray diffraction) with a Cu K α radiation source ($\lambda = 0.15418$ nm). The XRD data were collected using a step-scan mode with a step size of 0.02°, a goniometer speed of 6°/min

Table 1

Chemical composition of the base transparent glaze.

Oxide	SiO ₂	Al ₂ O ₃	CaO	MgO	K ₂ O	Na ₂ O	ZrO ₂	BaO	else	LOI
Content/%	59.75	12.07	9.86	1.95	2.38	2.33	1.36	4.67	0.93	4.70

and a scanning range (2θ) of 5–80°. Microstructures of the pigments and the glaze samples were investigated using a scanning electronic microscope (SEM, SU8010, Hitachi). The color glaze samples were etched by HF solution (5 wt%) before SEM test. Microstructures, high resolution transmission electron microscope images (HRTEM) and selected area electron diffraction (SEAD) were carried out using a transmission electron microscope (TEM, JEOL JEM-1010/2010, Japan). Thermal evolution process of the precursor was studied by simultaneous thermogravimetric and differential scanning calorimeter (DSC/TG, NETZSCH STA 449C). Analysis was conducted from room temperature to 1200 °C at a rate of 10 °C/min in air using α -Al₂O₃ as a reference. CIE lab parameters L^* , a^* , and b^* were measured using a spectrophotometer (Hunter Lab Miniscan MSXP 4000, 400–700 nm, white glazed tile reference $x = 31.5$, $y = 33.3$). Here, L^* is the lightness axis (black (0) ~ white (100)), b^* is the blue (–) ~ yellow (+) axis, and a^* is the green (–) ~ red (+) axis. ΔE is the hue variation and means the color difference between two products. Hue variation can be calculated by the following equation: $\Delta E = [(\Delta L^*)^2 + (\Delta a^*)^2 + (\Delta b^*)^2]^{1/2}$. The chemical stability of the pigment is characterized by acid and alkali resistance. The pigment was tested by soaking exactly weighed quantity of the pigments in 10 wt% HCl, 10 wt% HNO₃, 10 wt% H₂SO₄, 10 wt% NaOH solutions and water under magnetic stirring for 0.5 h at room temperature. The pigments were filtered, washed, dried and weighed. The weight and the color of the pigments before and after the check with acids and alkali were measured. UV–visible spectroscopy of the pigments and glaze samples were recorded using diffuse reflectance with an integrating sphere (Perkin-Elmer, USA) in the 200–900 nm range, with a step of 0.3 nm, and with BaSO₄ as a reference. Chemical composition of the transparent glaze was determined using an X-ray fluorescence spectrometer (Shimadzu, XRF-1800, Japan) that was equipped with a Rh target. The measurement for XRF is based on the melting method. The glaze was dried in an oven at 105 °C for 24 h to eliminate the moisture content prior to XRF analysis. The glaze mixed with the binder (starch) homogeneously after drying, and then the test block was formed by pressing the mixed powder in a stainless-steel mold under 20 Mpa of pressure. Finally, Loss of Ignition (LOI) was determined by heated at 1025 °C for 20min, and the chemical composition was determined by heated at 1150 °C for 20 min. Valence state of manganese (Mn), titanium (Ti) and oxygen (O) ions in the pigment was determined by X-ray photoelectron spectroscopy (Escalab 250Xi; Thermo Fisher Scientific, Waltham, MA, USA). The binding energy values were calibrated based on the C1s peak that was measured at 284.8 eV.

3. Results and discussion

Fig. 1 illustrates the DTA-TG curves of the precursor, which is a mixture of MnO and TiO₂. There are two stages of weight change in the precursor, and the total weight loss is only 0.39% after heating to 1200 °C. On the basis of the TG curve, the first weight change stage (room temperature~700 °C) is a weight gain process, which could be attributed to the oxidization of MnO to a high-valence manganese oxide species. After calculation and analysis, it may be Mn₂O₃ [19]. Of course, this needs to be further confirmed by XRD analysis. Additionally, the corresponding oxidation temperature is 565.0 °C in the DTA curve. The second stage is a weight loss process, which is from 700 to 1100 °C. In this stage, a sharp endothermic peak was observed at 990.1 °C in the DTA curve, which was ascribed to the formation of MnTiO₃. Meanwhile, the weight loss behavior is attributed to the reduction of trivalent Mn cation (Mn³⁺) to divalent Mn cation (Mn²⁺).

Fig. 2 exhibits XRD patterns of MnTiO₃ pigment calcinated at different temperatures. It can be seen that MnO is transformed into Mn₂O₃ (PDF-#41-1442) after calcination at 700 °C, which is consistent with the DTA-TG analysis in Fig. 1. As the temperature increases from 700 to 900 °C, the peaks of Mn₂O₃ gradually weaken. Nevertheless, no diffraction peaks of MnO or MnTiO₃ were detected, suggesting that the Mn₂O₃

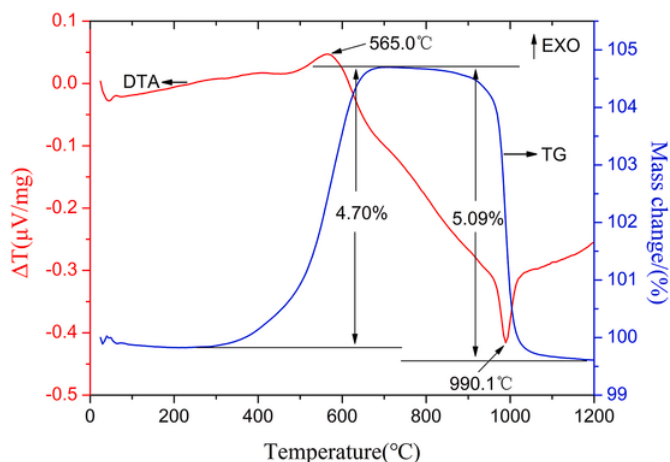


Fig. 1. DTA-TG curves of the precursor.

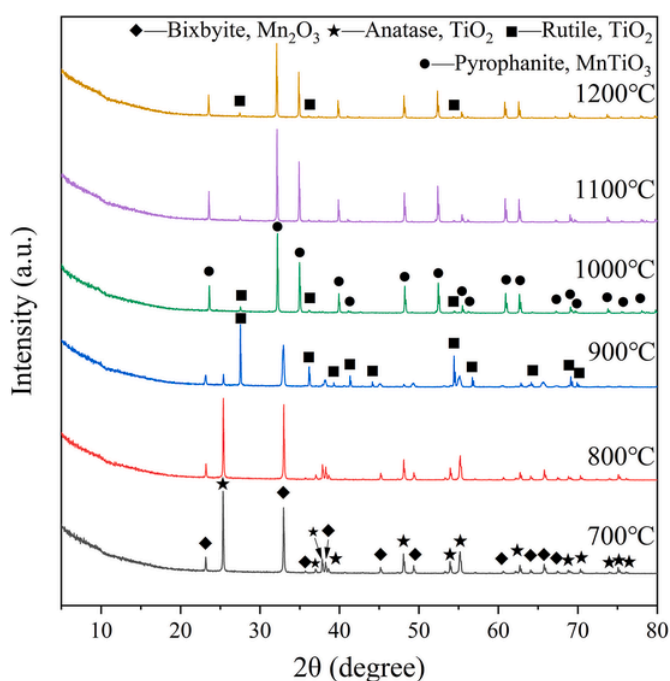
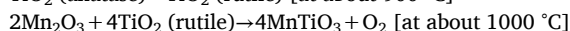
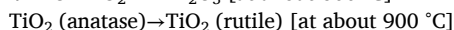
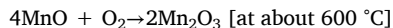


Fig. 2. XRD patterns of the MnTiO₃ pigments calcinated at different temperatures.

was not reduced to MnO before the reaction with TiO₂ to form MnTiO₃. Meanwhile, TiO₂ is transformed from anatase phase (PDF-#21-1272) to rutile phase (PDF-#21-1276) after calcination at 900 °C. When the calcination temperature reached 1000 °C, MnTiO₃ phase (PDF-#29-0902) is observed, and Mn₂O₃ phase is disappeared.

It should be noted that the synthesized MnTiO₃ pigment contains an impurity of TiO₂ (rutile), despite the initial reagents follow a strictly stoichiometric ratio. Furthermore, although the diffraction peaks of TiO₂ (rutile) disappeared in the samples with an initial Mn/Ti ratio greater than 1, Mn species other than MnTiO₃ were still not detected (as seen in Fig. S1). Considering that the melting points of MnO₂ and Mn₂O₃ are only 535 °C and 1080 °C, respectively, it speculates that the absence of Mn species should be attributed to the loss of manganese oxides through melting into a liquid phase. This is supported by the fact that the inner wall of the corundum crucible used for the synthesis of the MnTiO₃ pigments was dyed black/brown. Fortunately, loss of Mn species had little impact on the color properties of the MnTiO₃ pigments, as shown in Fig. S2.

So far, the formation process of MnTiO₃ can be deduced as follows:



To investigate the microstructure of the prepared MnTiO₃ pigment, the SEM and TEM analyses were carried out, as shown in Fig. 3. The SEM image from Fig. 3(a) demonstrates that the MnTiO₃ pigment shows an irregular morphology, which conforms to the morphological characteristics of the powder prepared by solid-state method [20]. In addition, particle size of MnTiO₃ pigment is in the range of 2–5 μm, suggesting that the pigment can be used directly into glaze without milling further [1]. Interestingly, many hexagonal layered structures were observed in the particle surface of MnTiO₃ pigment. Furthermore, the area of these hexagonal layered structure decreases gradually in the c-axis direction, indicating that the MnTiO₃ pigment particle is grown layer-by-layer from inside to outside. The HRTEM image in Figs. 3(b-2) exhibits the interplanar spacing of the prepared MnTiO₃ pigment is approximately 0.279 nm, close to the (104) lattice spacing of MnTiO₃. SEAD reflections found in this region can be assigned to the (124), (220) and (104) crystal planes of the hexagonal structure of space group R-3(148). Both of HRTEM and SEAD analysis demonstrate that the prepared MnTiO₃ pigment has high crystallinity.

Fig. 4 illustrates the chromatic parameters and photographs of MnTiO₃ pigments calcinated at different temperatures. As the calcination temperature increased from 800 to 1200 °C, the L*-value of MnTiO₃ pigment continuously decreased and then reached a minimum value at 1100 °C, which is only 25.85. Meanwhile, the a*- and b*-value are close to 0. Additionally, the photograph demonstrates that the MnTiO₃ pigment calcinated at 1100 °C shows the pure and deepest black hue. In order to highlight the advantages of the MnTiO₃ pigment reported in this work, the L*-values, synthesis methods and process parameters of different black pigments reported in recent literature were summarized in Table 2 [1-3,7-9,21-29]. Obviously, the L*-values of C@ZrSiO₄ black pigments are generally greater than 30, suggesting that the pigments show a dark grey, not black [7-9,21,22]. Meanwhile, C@ZrSiO₄ black pigments are usually prepared by liquid-phase method, such as non-hydrolytic sol-gel method, sol-gel-spraying, and so on. The complex preparation process and expensive raw materials, e.g., ZrCl₄, TEOS, C₆H₁₂N₄, will lead to high cost of C@ZrSiO₄ pigment. Besides, an inert gas, e.g., N₂ or Ar, is essential for preparing C@ZrSiO₄ pigment, which can prevent the oxidation of the carbon source used as colorant [1,7-9,21-23]. It has put forwards higher requirements on the production equipment and cost control of C@ZrSiO₄ pigment. On the other hand, a complex chemical composition, expensive raw materials, higher synthesis temperature and longer holding time are the defects of metallic oxide-based black pigments [2,3,24-29]. To sum up, compared with C@ZrSiO₄ pigment and metallic oxide-based black pigments, the MnTiO₃ black pigment prepared by solid-state method has many advantages, for instance superior color performance (L* = 25.85, a* = 3.86, b* = 0.91), simple chemical composition, facile preparation route and low production cost, etc.

To further investigate the color behavior of MnTiO₃ pigment, UV-vis absorption analysis was performed, whose results are shown in Fig. 5. It can be seen that the MnTiO₃ pigment calcined at 1100 °C has the strongest absorption intensity in the full visible light region (380–780 nm), indicating that the pigment shows the deepest black hue, which is consistent with the results of chromatic parameters [30]. Thereinto, the strongest absorption band at λ = 516 nm, corresponding to green-light region, with an absorption intensity of 86.74%. The UV-Vis spectra of the MnTiO₃ pigment shows a wide absorption band in the full visible light region, which was assigned to the ⁶A_{1g} → ⁴A_{1g} and ⁶A_{1g} → ⁴T_{2g} crystal field transition of octahedral Mn²⁺ site [17,18]. Besides, the light absorption intensity in the red-light region is weaker

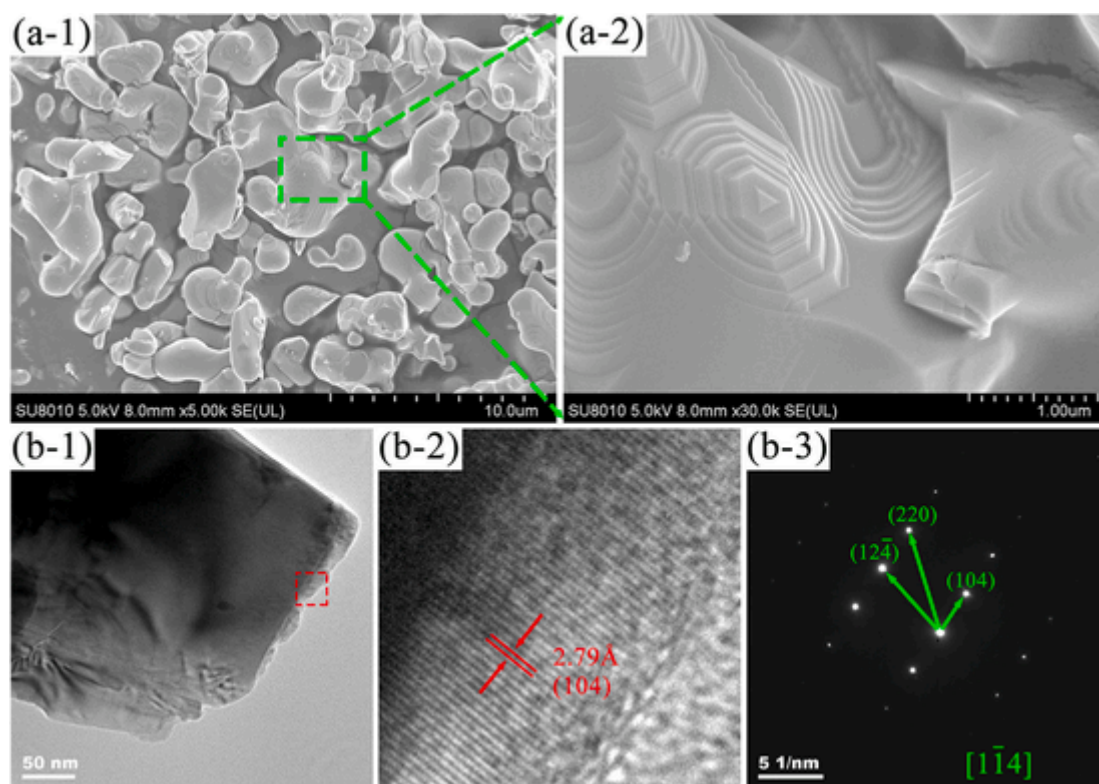


Fig. 3. SEM images (a-1 and a-2), TEM image (b-1), HRTEM (b-2) and SEAD pattern (b-3) of MnTiO_3 pigment. (Note: calcination temperature is 1100°C).

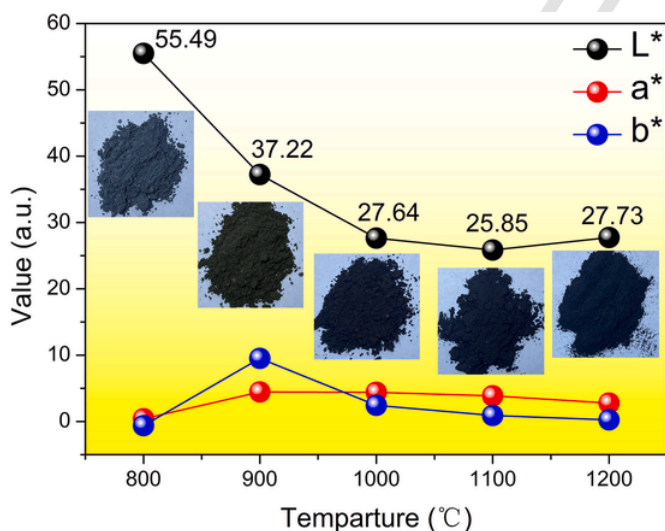


Fig. 4. Chromatic parameters and photographs of MnTiO_3 pigments calcinated at different temperatures.

compared to the other light region, which leads to an a^* -value greater than 0 ($a^* = 3.86$).

In our previous research, the composition and chemical states on the particle surface have already been shown to have a significant impact on color properties of ceramic pigment [31,32]. In order to determine the surface information of MnTiO_3 pigment, XPS analysis was performed. Fig. 6(a) displays the survey spectrum of MnTiO_3 pigment surface, which suggests only the existence of Mn, Ti and O elements in the prepared pigment surface, and no peaks related to other elements is detected. The charge effect was corrected by aligning the C element at 284.8 eV [31]. The peaks are located at approximately 642, 457 and 529 eV were detected, which were ascribed to Mn 2p, Ti 2p and O 1s,

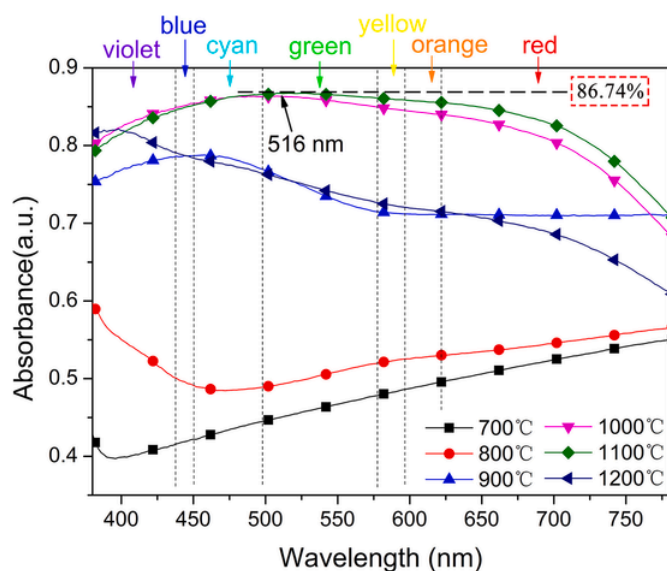
respectively. Fig. 6(b) illustrates the high-resolution XPS spectrum of Mn 2p, which consisted of four peaks at binding energy of 640.03, 641.55, 651.77 and 653.31 eV [15]. According to the previous reports, two signals at 640.03 and 651.77 eV were assigned to divalent Mn cation (Mn^{2+}), while two signals at 641.55 and 653.31 eV were assigned to trivalent Mn cation (Mn^{3+}). Besides, the peak at 645.62 eV was ascribed to a satellite peak. Consequently, it can be concluded that Mn cations in the MnTiO_3 pigment surface has two valence states, i.e., divalent (+2) and trivalent (+3), rather than only +2. Moreover, the occupation ratio of $\text{Mn}^{2+}/\text{Mn}^{3+}$ is 1.50. Fig. 6(c) presents the high-resolution XPS spectrum of Ti 2p, which consisted of two peaks at binding energy of 457.76 and 463.39 eV. The two signals correspond to the $\text{Ti}^{4+} 2p_{3/2}$ and $\text{Ti}^{4+} 2p_{1/2}$ feature peaks, related to the octahedrally coordinated Ti^{4+} in MnTiO_3 lattice, indicating that tetravalent (+4) is the only valence state of Ti element in MnTiO_3 . Fig. 6(d) shows the O 1s region fitted with three peaks located at 529.31 and 530.63 eV, which were assigned to the Ti–O and Mn–O bonds in the MnTiO_3 crystal structure, suggesting that Mn and Ti atoms are connected by bridging oxygen. In addition, the peak located at 532.04 eV was ascribed to adsorbed- O_2 on the pigment surface. More importantly, the atomic ratio of Mn/Ti is 0.87, not the stoichiometric ratio (i.e., 1). This could be explained by the presence of dislocations or defects such as oxygen and manganese vacancies in MnTiO_3 lattice. A similar phenomenon was also observed in the SrTiO_3 lattice [15,33].

Based on the above results, it can be seen that the content of Mn^{2+} on the pigment surface is a key factor affecting the color property of the MnTiO_3 pigment. In view of this, the $\text{Mn}^{2+}/\text{Mn}^{3+}$ ratios of the MnTiO_3 pigment surfaces calcinated at 1000°C and 1200°C were also calculated by XPS analysis, respectively. Fig. 7 compares the effect of synthesis temperature on the $\text{Mn}^{2+}/\text{Mn}^{3+}$ ratio in the MnTiO_3 pigment surfaces. As expected, the sample with the best color performance (1100°C) had the highest $\text{Mn}^{2+}/\text{Mn}^{3+}$ ratio on particle surfaces, i.e., the highest Mn^{2+} content.

Chemical stability is very important for the application of pigment. To survey the chemical stability of the MnTiO_3 pigment, the acid, alkali

Table 2Comparison of the L^* -values, synthesis methods, synthesis temperatures and holding times of different black pigments.

Pigment	L^* -value	Synthesis method	Temperature (°C)	Holding time (h)	Ref.
C@ZrSiO ₄	39.09	non-hydrolytic sol-gel	950	2	[7]
	33.08	molten-salt assisted	1000	2	[21]
	34.93	non-hydrolytic sol-gel	950	2	[9]
	33.02	non-hydrolytic sol-gel	950	2	[9]
	42.01	non-hydrolytic sol-gel	900	2	[8]
	41.04	non-hydrolytic sol-gel	900	2	[22]
	22.21	liquid-phase	1050	2	[23]
	19	sol-gel-spraying	1150	3	[1]
	La _{0.6} Ca _{0.4} CoO ₃	36.19	polymeric precursor	800	3
(Fe _x Cr _{1-x}) ₂ O ₃	23.13	solid state	1200	2	[25]
Fe _{0.7} Cr _{1.3} O ₃ /FePO ₄	23.84	solid state	1000	2	[26]
CoFe _{1.7} Cr _{0.3} O ₄	9	solid state	1200	1	[27]
Ni _{0.925} Mn _{0.075} Fe _{1.375} Cr _{0.5} Mn _{0.125} O ₄	10	solid state	1200	1	[27]
CuFe ₂ O ₄	37.55	polymeric precursor	700	4	[28]
Co _{2/3} Mn _{2/3} Fe _{2/3} Cr _{1.0} O ₄	39.6	solid state	1300	12	[2]
CoFe ₂ O ₄	29.76	conventional	1200	3	[29]
CoFe ₂ O ₄	22.72	co-precipitation	800	6	[29]
Fe–Cr–Mn spinel	39.7	–	–	–	[3]
Commercial black pigment-1	48.77	–	–	–	–
Commercial black pigment-2	39.43	–	–	–	–
MnTiO ₃	25.85	solid state	1100	1	This work

**Fig. 5.** UV-vis absorption spectra of MnTiO₃ pigments calcinated at different temperatures.

and water resistance were tested. As shown in Table 3, the weight loss of all samples was less than 2.0%. Considering the operating error, such weight loss could be neglected, which indicates that the MnTiO₃ pigment is stable and resistant to the different mineral acids and alkalis. The color difference (ΔE) is a common way for measuring the color difference between two pigments. The difference between two colors can be differentiated by the human eye when the value of the color difference is larger than 1 [34]. Table 3 demonstrates the color difference of MnTiO₃ pigment after treated by water, alkali and acid. Smaller ΔE values (all less than 1) also manifest that the synthesized MnTiO₃ pigment has outstanding chemical stability [35].

Ceramic glaze is the primary application scenario of ceramic pigment, so it is necessary to explore the tinting performance of the MnTiO₃ pigment in ceramic glaze [8,32]. Fig. 8 exhibits the photographs of color glaze samples with different MnTiO₃ pigment additions. As the addition of MnTiO₃ pigment increased, the differences in

color of glaze samples were observed. Obviously, the glaze sample without MnTiO₃ (control group) is white, while the MnTiO₃-containing samples have a comparatively strong coloration, which can be seen in the lower L^* -values. As the pigment addition increased from 0 to 12 wt%, the L^* -values of color glaze samples were continuously decreased and then reached a minimum value at the addition of 8 wt%, which is 11.44. Intuitively, samples with the pigment addition less than 6 wt% are brownness, those whose pigment addition of 8–10 wt% show black, and the ones added 12 wt% pigment is pale brown. The glaze samples with pigment addition less than 8 wt% had superior surface gloss and no defect was observed, suggesting that the MnTiO₃ pigment has outstanding high temperature stability, chemical stability and chemical compatibility with base transparent glaze [31,36]. It should be noted that the color performance of the color glaze samples starts to deteriorate when the pigment addition exceeds 8 wt%, for example the black hue is diminished and the glazes lose their vitreous luster.

In order to further elaborate the advantages of the MnTiO₃ pigment, Table 4 compares the L^* -values and additive amounts of black glazes colored with different black pigments. It is obvious that 11.44 is the minimum L^* -value reported in the current literature [1–3,23,25]. Moreover, the additive amount of MnTiO₃ pigment is significantly less than that of C@ZrSiO₄ pigment [1,23]. By contrast, the additive amount of MnTiO₃ pigment is only slightly higher than that of the metallic oxide-based black pigments [2,3,25]. Considering the lower price of the MnTiO₃ pigment, the extra additive amounts are negligible.

UV-vis absorption spectrum allows a more accurate characterize the color behavior of the color glaze samples, as shown in Fig. 9. It is clear that the absorption intensity of the control group sample in the full visible light region is almost 0, so the sample is white. Conversely, the glaze sample with pigment addition of 8 wt% has the strongest light absorption intensity in the full visible light region, thereby this sample has the deepest hue. When the addition exceeds 8 wt%, the light absorption intensity of the glaze samples is weakened. Similarly, glaze samples show a weak absorbance in the yellow-red wavelengths at 580–780 nm when the pigment addition is less than 8 wt%. In brief, the addition amount of MnTiO₃ pigment has a great influence on the color properties of color glaze, and the glaze shows a dark black when the pigment addition is 8 wt%. This color evolution behavior is related to the tinting mechanism of MnTiO₃ pigment.

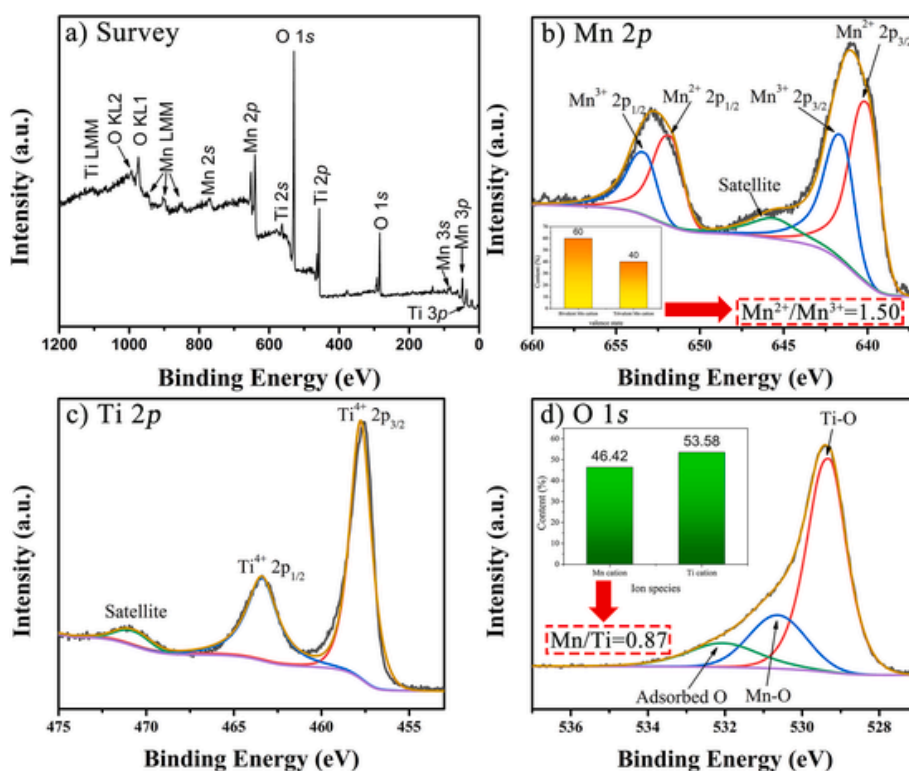


Fig. 6. Survey spectrum (a) and high-resolution XPS spectra of (b) Mn 2p, (c) Ti 2p and (d) O 1s core levels for MnTiO₃ pigment calcinated at 1100 °C.

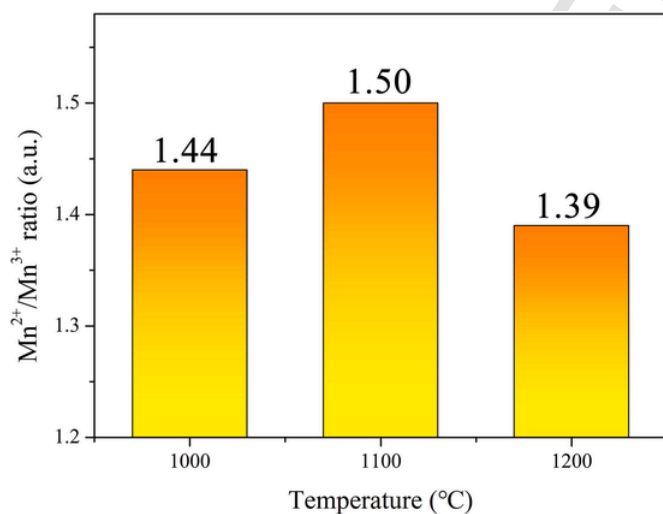


Fig. 7. Mn²⁺/Mn³⁺ ratios on the surface of the MnTiO₃ pigments calcinated at different temperatures.

Table 3
Chromatic values of MnTiO₃ pigment after water, acid and alkali tests.

Acid/Alkali	MnTiO ₃				
	L*	a*	b*	ΔE	weight loss (%)
In air	25.33	3.63	0.88	–	–
H ₂ O	25.12	4.02	0.97	0.45	1.2
HNO ₃	25.41	3.48	0.37	0.54	1.2
HCl	25.79	3.52	0.32	0.73	1.8
H ₂ SO ₄	24.91	3.70	0.81	0.43	1.0
NaOH	25.04	3.50	0.27	0.69	0.2

Fig. 10 presents the XRD patterns of color glaze samples with different MnTiO₃ pigment additions. It is observed that all samples are amorphous, which the characteristic diffuse peak centered at $2\theta \approx 29^\circ$. Meanwhile, diffraction peaks corresponding to other crystalline phases were also observed. For instance, a weak peak corresponding to the quartz (PDF-#46-1045) was detected in the control group. In contrast, the ZrSiO₄ phase (PDF-#06-0266) was detected in the MnTiO₃-containing samples. Combined with the chemical composite of the base transparent glaze (Table 1), it can be inferred that the zirconium and silicon species of ZrSiO₄ are sourced from base transparent glaze, and the addition of MnTiO₃ pigment promotes ZrSiO₄ phase formation. It is important that no diffraction peak of MnTiO₃ is detected in the MnTiO₃-containing samples, suggesting that MnTiO₃ pigment has been melted into the base transparent glaze. It was therefore concluded that the tinting mechanism of MnTiO₃ pigment is “ion tinting”, which means the color source of MnTiO₃-containing glaze derived from Mn cations melted in the glass phase, instead of MnTiO₃ crystals [37]. Consequently, the color of MnTiO₃-containing glaze is determined by the Mn cation concentration in the glass phase. Similarly, 8 wt% MnTiO₃-containing glaze showing deep black hue is attributed to the high Mn²⁺ content in the glass phase.

Based on the tinting mechanism of MnTiO₃ pigment, it is conceivable that the color of glaze should be darker and darker with the amount of pigment added to base glaze increases, whereas this is not the case. In order to clarify the reasons, the microstructures of glaze samples with different MnTiO₃ pigment added was investigated. Fig. 11 presents the SEM images of the color glaze samples with 0 wt%, 4 wt%, 8 wt% and 12 wt% MnTiO₃ pigment, respectively. Obviously, the MnTiO₃ addition has a great effect on the microstructure of glaze. The size of the constituent particles gradually increases with the increase of the MnTiO₃ addition. It has been reported in the literature that titanium-containing oxide would be highly soluble in glaze melts at high temperature and may participate in forming the glaze network in the form of [TiO₄] tetrahedral coordination. However, partial Ti⁴⁺ will get off from the network and transform into a stable structure of [TiO₆] oc-

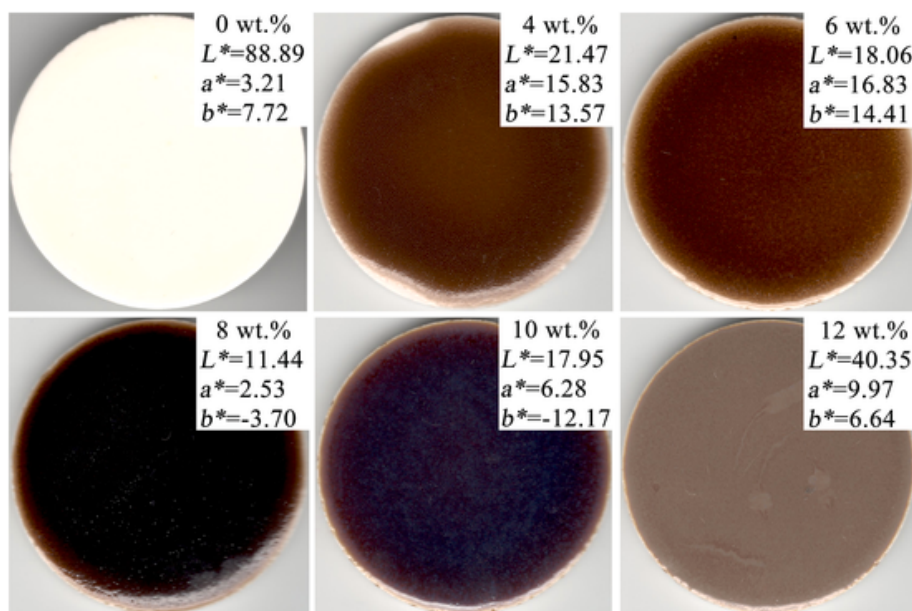


Fig. 8. Digital images of color glaze samples with different MnTiO_3 pigment additions. (For interpretation of the references to color in this figure legend, the reader is referred to the Web version of this article.)

Table 4

Comparison of the L^* -values and additive amounts for the black glaze using different black pigments.

Pigment	additive amount (wt.%)	L^* -value	Ref.
C@ZrSiO ₄	10	29.58	[23]
C@ZrSiO ₄	30	33.47	[1]
Co _{2/3} Mn _{2/3} Fe _{2/3} Cr _{1.0} O ₄	–	28.3	[2]
Fe–Cr–Mn spinel	5	27.7	[3]
Cr–Ni–Cu metallic oxide	5	17.6	[3]
(Fe _x Cr _{1-x}) ₂ O ₃	5	14.19	[25]
MnTiO ₃	8	11.44	This work

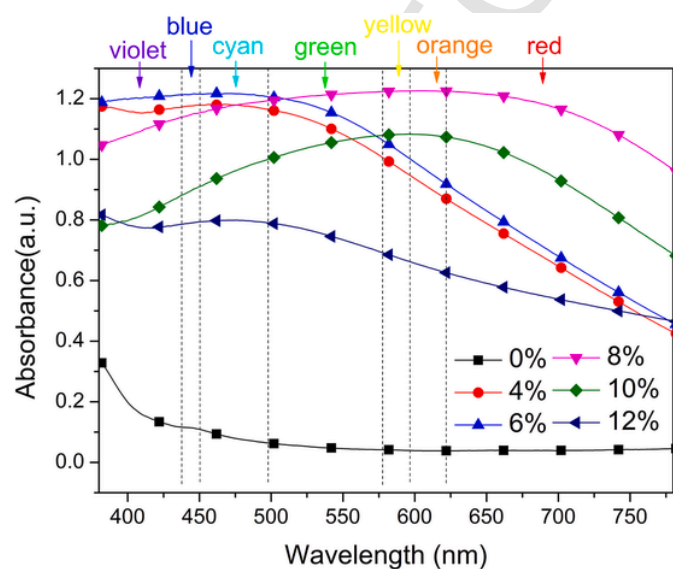


Fig. 9. UV-vis absorption spectra of color glaze samples with different MnTiO_3 pigment additions. (For interpretation of the references to color in this figure legend, the reader is referred to the Web version of this article.)

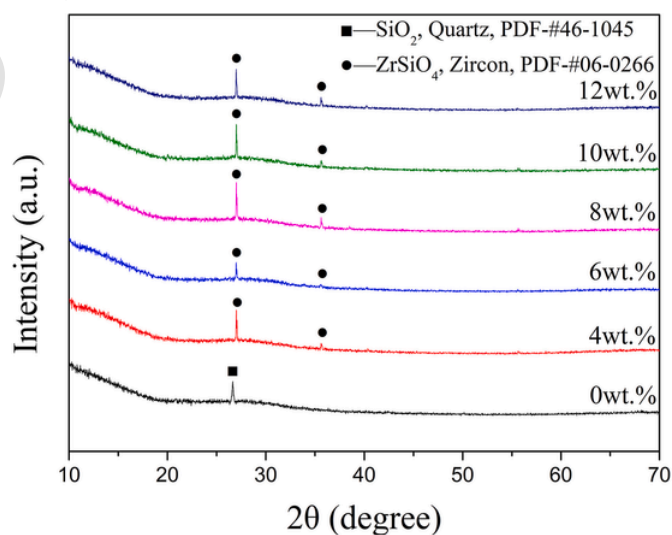


Fig. 10. XRD patterns of color glaze samples with different MnTiO_3 pigment additions. (For interpretation of the references to color in this figure legend, the reader is referred to the Web version of this article.)

tahedral coordination at low temperature. The freed Ti^{4+} will bond with other network modifier (Ca^{2+} , Mg^{2+} , Zn^{2+} etc.) to induce phase separation phenomenon. Therefore, the introducing of TiO_2 can promote the phase-separation and then the size of separated nanoparticle increases [38,39].

As can be seen in Fig. 11(a and b), the based glaze (i.e., control group sample) and 4 wt% MnTiO_3 -containing glaze are composed of a large number of nanoparticles with a size of about 10–30 nm. The size of these nanoparticles is much smaller than the visible light wavelength, so they do not interfere with the propagation of light [40,41]. As a result, the control group sample and the 4 wt% MnTiO_3 -containing glaze are transparent. In contrast, the glaze appearance changes from a transparency to a weak opacification, when adding 8 wt% MnTiO_3 , as shown in Fig. 11(c). Meanwhile, a worm-like phase-separated structure with a size of about 100 nm was formed in the 8 wt% MnTiO_3 -containing glaze. It should be noted that the phase-separated structure

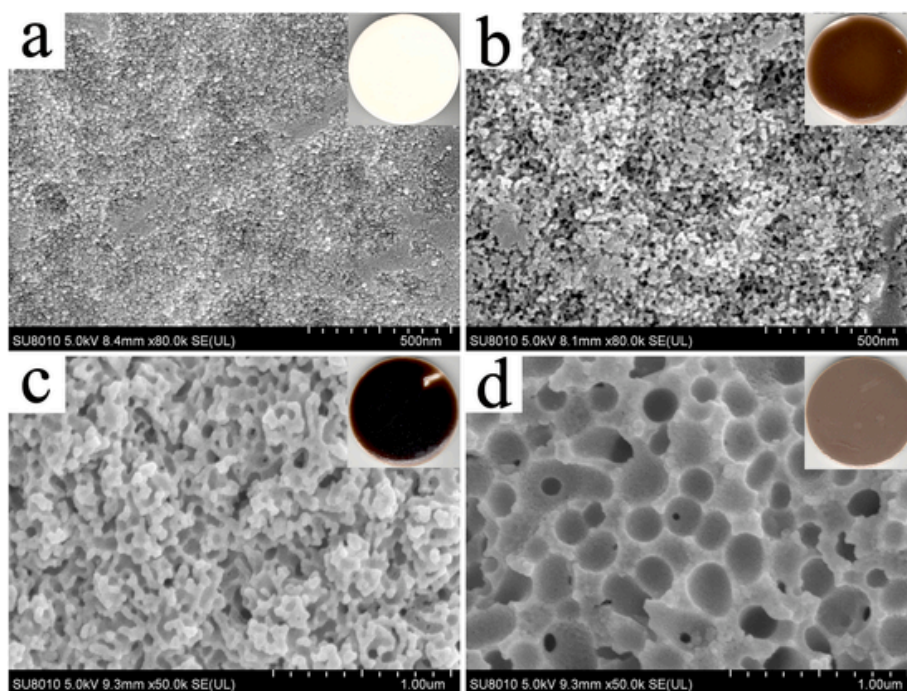


Fig. 11. SEM images of the color glaze samples with 0 wt% (a), 4 wt% (b), 8 wt% (c) and 12 wt% (d) MnTiO_3 pigment, respectively. (For interpretation of the references to color in this figure legend, the reader is referred to the Web version of this article.)

can produce structural color [42]. Moreover, the Rayleigh scattering ($d \leq 100$ nm) could be formed when the size of the phase-separated structure is less than 100 nm, which gave rise to the blue opalescence [43,44]. Consequently, this sample lost its transparency and had a blue hue, as evidenced by the negative b^* -value (-3.70) [37]. Combined with the tinting effect of high concentration of Mn ions, the 8 wt% MnTiO_3 -containing glaze shows black hue. For the 12 wt% MnTiO_3 -containing glaze sample, a discrete droplet liquid-liquid phase-separated structures with a size of about 200 nm were appeared. It means that the Mie scattering ($d > 100$ nm) could be formed, which gave rise to the milk white [44]. Therefore, this sample shows opaque brown hue. Analogously, it is precisely because of the milk white produced by the Mie scattering that the color of the glaze gradually lightens when the addition of MnTiO_3 pigment exceeds 8 wt%. To sum up, MnTiO_3 black pigment can give transparent glaze an excellent deep black, but the addition needs to be strictly controlled.

MnTiO_3 black pigment can also be used as raw materials for coating that absorb solar energy, in addition to being used as a colorant for ceramic glaze. Fig. 12(a) exhibits the photograph of the MnTiO_3 pigmented coating. The coating has a better surface quality, such as the flatness, indicating that the MnTiO_3 pigment has good compatibility with acrylic paints. And then, MnTiO_3 pigment was used as the solar absorbing material, and its solar energy utilization performance was evaluated by measuring the temperature change of the MnTiO_3 pigmented coating, the control group and the coatings prepared using commercial black pigments were presented in Fig. 12(b). It is obvious that the temperature of MnTiO_3 pigmented coating is the highest after illumination by an infrared lamp (simulated solar source) compared to the other coating samples. The results show that the MnTiO_3 pigment has an outstanding solar energy utilization performance, and showing its promising application in solar absorber [45].

4. Conclusion

To summarize, this article synthesized an overlooked black pigment, MnTiO_3 , via a solid-state route. Meanwhile, color properties and tinting

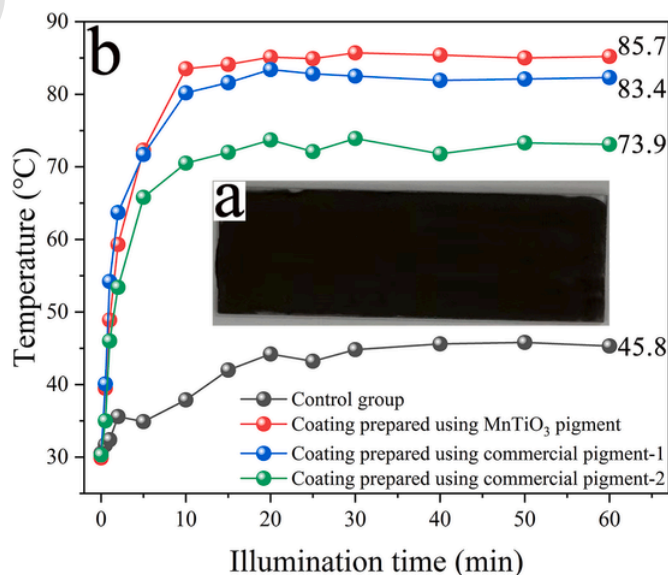


Fig. 12. (a) A photograph of the coating prepared using MnTiO_3 pigment, (b) Temperature curves of coatings prepared using different pigments illuminated by an infrared lamp.

performance of MnTiO_3 pigment were investigated. The main conclusions are as follow:

- (1) The MnTiO_3 pigment showed a pure and deep black hue, whose chromatic parameters are $L^* = 25.85$, $a^* = 3.86$ and $b^* = 0.91$, respectively. Compared with other kinds of black pigments, MnTiO_3 pigment has many advantages such as simple chemical composition, facile preparation craft, low cost, and so on.
- (2) There are two valence states for Mn cations on the surface of the MnTiO_3 pigment, divalent (+2) and trivalent (+3). Simultaneously, the Mn/Ti ratio exhibits a non-stoichiometric

ratio. The color mechanism of MnTiO₃ black pigment is attributed to its super-strong light absorption intensity in the full visible light region, and the light absorption mechanism was ascribed to the ⁶A_{1g}→⁴A_{1g} and ⁶A_{1g}→⁴T_{2g} crystal field transition of octahedral Mn²⁺ site.

- (3) MnTiO₃ pigment shows an excellent tinting performance. The L*-value of the 8 wt% MnTiO₃-containing glaze sample is only 11.44, which is the minimum L*-value reported in the literature. For ceramic glaze, the tinting mechanism of MnTiO₃ pigment is “ion tinting”, thereby the color performance of the MnTiO₃-containing glaze is positively correlated with the addition of MnTiO₃ pigment. However, excessive MnTiO₃ pigment can lead to deterioration of the color performance of glaze, due to overmuch Ti could lead to the formation of a phase-separated structure in the glaze.
- (4) MnTiO₃ pigment can be used as raw materials for coating. Moreover, the MnTiO₃ pigmented coating shows an outstanding solar energy utilization performance.

CRedit authorship contribution statement

Qikun Wang : Conceptualization, Formal analysis, Writing – original draft. **Fanbing Lai** : Investigation, Data curation. **Weishi Shi** : Resources, Methodology, Data curation. **Xiaohong Li** : Resources. **Renhua Chen** : Resources. **Huafeng Liu** : Resources. **Xiaozhen Zhang** : Resources, Formal analysis. **Qibing Chang** : Funding acquisition, Resources, Supervision. **Yongqing Wang** : Funding acquisition, Supervision, Writing – review & editing.

Declaration of competing interest

The authors declare that they have no known competing financial interests or personal relationships that could have appeared to influence the work reported in this paper.

Data availability

Data will be made available on request.

Acknowledgements

The authors gratefully acknowledge the financial support by the National Natural Science Foundation of China (Nos. 21761015, 51772136), Jiangxi Provincial key research and development program (20202BBE53011), Science Foundation of Jiangxi Provincial (P. R. China) Department of Education (Nos. GJJ211317).

Appendix A. Supplementary data

Supplementary data to this article can be found online at <https://doi.org/10.1016/j.matchemphys.2023.127310>.

References

- Q. Chang, X. Wang, Y. Wang, Q. Bao, J.-e. Zhou, Q. Zhu, Encapsulated carbon black prepared by sol-gel-spraying: a new black ceramic pigment, *J. Eur. Ceram. Soc.* 34 (2014) 3151–3157.
- M. Dondi, C. Zanelli, M. Ardit, G. Cruciani, L. Mantovani, M. Tribaudino, G.B. Andreozzi, Ni-free, black ceramic pigments based on Co—Cr—Fe—Mn spinels: a reappraisal of crystal structure, colour and technological behaviour, *Ceram. Int.* 39 (2013) 9533–9547.
- C. Gargori, S.R. Prim, M. Llusar, M.V. Folgueras, G. Monrós, Recycling of Cr/Ni/Cu plating wastes as black ceramic pigments, *Mater. Lett.* 218 (2018) 341–345.
- E. Ozel, S. Turan, Production and characterisation of iron-chromium pigments and their interactions with transparent glazes, *J. Eur. Ceram. Soc.* 23 (2003) 2097–2104.
- S. Chen, S. Fu, Y. Lang, C. Tian, H. Wei, C.-A. Wang, Submicronic spherical inclusion black pigment by double-shell reaction sintering, *J. Am. Ceram. Soc.* 103 (2020) 1520–1526.
- H. Tang, Q. Hu, F. Jiang, W. Jiang, J. Liu, T. Chen, G. Feng, T. Wang, W. Luo, Size control of C@ZrSiO₄ pigments via soft mechano-chemistry assisted non-aqueous sol-gel method and their application in ceramic glaze, *Ceram. Int.* 45 (2019) 10756–10764.
- T. Chen, X. Zhang, W. Jiang, J. Liu, W. Jiang, Z. Xie, Synthesis and application of C@ZrSiO₄ inclusion ceramic pigment from cotton cellulose as a colorant, *J. Eur. Ceram. Soc.* 36 (2016) 1811–1820.
- W. Jiang, X. Xu, T. Chen, J. Liu, X. Zhang, Preparation and chromatic properties of C@ZrSiO₄ inclusion pigment via non-hydrolytic sol-gel method, *Dyes Pigments* 114 (2015) 55–59.
- T. Chen, X. Zhang, W. Jiang, J. Liu, Z. Xie, W. Jiang, Preparation of plant derived carbon and its application for inclusion pigments, *Adv. Powder Technol.* 29 (2018) 3040–3048.
- L. Yuan, A. Han, M. Ye, X. Chen, L. Yao, C. Ding, Synthesis and characterization of environmentally benign inorganic pigments with high NIR reflectance: lanthanum-doped BiFeO₃, *Dyes Pigments* 148 (2018) 137–146.
- Q. Wang, Y. Wang, K. Liu, J. Liu, C. Wang, Y. Wang, Q. Chang, High-performance spherical urchin-like CoAl₂O₄ pigments prepared via microemulsion-hydrothermal-precipitation method, *Adv. Powder Technol.* 31 (2020) 1290–1301.
- W. Dong, D. Wang, L. Jiang, H. Zhu, H. Huang, J. Li, H. Zhao, C. Li, B. Chen, G. Deng, Synthesis of F doping MnTiO₃ nanodisks and their photocatalytic property under visible light, *Mater. Lett.* 98 (2013) 265–268.
- R.A.P. Ribeiro, J. Andrés, E. Longo, S.R. Lazaro, Magnetism and multiferroic properties at MnTiO₃ surfaces: a DFT study, *Appl. Surf. Sci.* 452 (2018) 463–472.
- R.K. Maurya, D. Singh, Nano-mechanical behavior of MnTiO₃ ceramics, *Mater. Lett.* 246 (2019) 49–51.
- C. Koop-Santa, A. Sanchez-Martinez, E.R. López-Mena, J.L.A. Ponce-Ruiz, E. Orozco-Guareño, O. Ceballos-Sanchez, Physicochemical properties of MnTiO₃ powders obtained by molten salt method, *Ceram. Int.* 47 (2021) 33315–33321.
- X. Lu, C. Chen, W. Zhu, H. Wu, Y. Hou, J. Zhang, F. Huang, X. Lu, J. Zhu, Effect of oxygen vacancy on the magnetic and electric properties in MnTiO₃ ceramics, *Mater. Lett.* 155 (2015) 71–74.
- Z.-Q. Song, S.-B. Wang, W. Yang, M. Li, H. Wang, H. Yan, Synthesis of manganese titanate MnTiO₃ powders by a sol-gel-hydrothermal method, *Mat. Sci. Eng. B-Adv.* 113 (2004) 121–124.
- G.W. Zhou, Y.S. Kang, Synthesis and structural properties of manganese titanate MnTiO₃ nanoparticle, *Mat. Sci. Eng. C-Mater.* 24 (2004) 71–74.
- W. Fu, T. Liu, S. Hou, Y. Guo, C. Mei, L. Zhao, Engineering MnO/C microsphere for enhanced lithium storage, *J. Alloys Compd.* 861 (2021) 157961.
- L.T.T. Vien, N. Tu, M.T. Tran, N. Van Du, D.H. Nguyen, D.X. Viet, N.V. Quang, D.Q. Trung, P.T. Huy, A new far-red emission from Zn₂SnO₄ powder synthesized by modified solid state reaction method, *Opt. Mater.* 100 (2020) 109670.
- T. Chen, X. Zhang, W. Jiang, Z. Xie, Y. Xu, H. Tang, W. Jiang, Molten-salt assisted synthesis and characterization of ZrSiO₄ coated carbon core-shell structure pigment, *Adv. Powder Technol.* 31 (2020) 2197–2206.
- X. Zhang, T. Chen, W. Jiang, J. Liu, Y. Xu, Z. Xie, Facile synthesis of tunable polymer spheres for encapsulation pigment application, *Mater. Lett.* 216 (2018) 63–66.
- S. Chen, M. Cheng, Y. Lang, H. Wei, C.-A. Wang, Synthesis and chromatic properties of zircon encapsulated ceramic black pigment with carbon sphere as carbon source, *J. Eur. Ceram. Soc.* 38 (2018) 2218–2227.
- D. Melo, F.T.G. Vieira, T.C.C. Costa, L.E.B. Soledade, C.A. Paskocimas, D.M.A. Melo, E. Longo, E.P. Marinho, A.G. Souza, I.M.G. Santos, Lanthanum cobaltite black pigments with perovskite structure, *Dyes Pigments* 98 (2013) 459–463.
- M. Du, Y. Du, Z. Chen, Z. Li, K. Yang, X. Lv, Y. Feng, Synthesis and characterization of black ceramic pigments by recycling of two hazardous wastes, *Appl. Phys. A-Mater.* 123 (2017) 575.
- L. Matović, R. Vujanin, K. Kumrić, S. Krstić, Y.-n. Wu, D.M. Kabtamu, A. Devečerski, Designing of technological scheme for conversion of Cr-rich electroplating sludge into the black ceramic pigments of consistent composition, following the principles of circular economy, *J. Environ. Chem. Eng.* 9 (2021) 105038.
- J.-H. Lee, J.-W. Kweon, W.-S. Cho, J.-H. Kim, K.-T. Hwang, H.-J. Hwang, K.-S. Han, Formulation and characterization of black ceramic ink for a digital ink-jet printing, *Ceram. Int.* 44 (2018) 14151–14157.
- A.F. Costa, P.M. Pimentel, F.M. Aquino, D.M.A. Melo, M.A.F. Melo, I.M.G. Santos, Gelatin synthesis of CuFe₂O₄ and CuFeCrO₄ ceramic pigments, *Mater. Lett.* 112 (2013) 58–61.
- H. Yüngeris, E. Ozel, Effect of the milling process on the properties of CoFe₂O₄ pigment, *Ceram. Int.* 39 (2013) 5503–5511.
- Q. Wang, Q. Chang, Y. Wang, X. Wang, J.-e. Zhou, Preparation of zircon-encapsulated carbon black ceramic pigment using the collapsed mesoporous-structure, *Silicon-Neth* 10 (2018) 2253–2262.
- Y. Wang, F. Lai, Q. Wang, Q. Long, C. Wang, W. Zhang, Q. Chang, Synthesis and chromatic properties of high color performance Pr_x-ZrSiO₄ (x = 0–0.1) yellow pigment, *J. Alloys Compd.* 891 (2022) 161932.
- W. Zhang, Q. Wang, X. Chen, X. Li, Q. Long, C. Wang, K. Liu, Y. Wang, Q. Chang, Synthesis of high color performance V-ZrSiO₄ blue pigment with low doping amount via inorganic sol-gel route, *Adv. Powder Technol.* 32 (2021) 3355–3363.
- K. Takehara, Y. Sato, T. Tohei, N. Shibata, Y. Ikuhara, Titanium enrichment and strontium depletion near edge dislocation in strontium titanate [001]/(110) low-angle tilt grain boundary, *J. Mater. Sci.* 49 (2014) 3962–3969.
- A.A. Ali, E. El Fadaly, I.S. Ahmed, Near-infrared reflecting blue inorganic nanopigment based on cobalt aluminate spinel via combustion synthesis method, *Dyes Pigments* 158 (2018) 451–462.
- W. Bao, F. Ma, Y. Zhang, X. Hao, Z. Deng, X. Zou, W. Gao, Synthesis and

- characterization of Fe³⁺ doped Co_{0.5}Mg_{0.5}Al₂O₄ inorganic pigments with high near-infrared reflectance, *Powder Technol.* 292 (2016) 7–13.
- [36] T. Chen, J. Zha, X. Zhang, X. Hu, W. Jiang, Z. Xie, W. Jiang, Synthesis and characterization of Pr_xZr_{1-x}SiO₄ (x = 0–0.08) yellow pigments via non-hydrolytic sol-gel method, *J. Eur. Ceram. Soc.* 38 (2018) 4568–4575.
- [37] Q. Wang, Q. Chang, Y. Wang, X. Wang, J.-e. Zhou, Ultrafine CoAl₂O₄ ceramic pigment prepared by Pechini-sacrificial agent method, *Mater. Lett.* 173 (2016) 64–67.
- [38] H. Zhan, C. Wu, C. Deng, X. Li, Z. Xie, C. Wang, Z.-g. Chen, Formation mechanism of titania based opacified glaze with novel core-shell nanostructure, *J. Eur. Ceram. Soc.* 39 (2019) 1668–1674.
- [39] K. Pekkan, The thermal and microstructural behavior of a R₂O–RO–(ZnO)–Al₂O₃–(TiO₂)–SiO₂ based macro-crystalline raw glaze system, *Ceram. Int.* 41 (2015) 7881–7889.
- [40] S. Wang, X. Li, C. Wang, M. Bai, X. Zhou, X. Zhang, Y. Wang, Anorthite-based transparent glass-ceramic glaze for ceramic tiles: preparation and crystallization mechanism, *J. Eur. Ceram. Soc.* 42 (2022) 1132–1140.
- [41] A.R. Molla, A.M. Rodrigues, S.P. Singh, R.F. Lancelotti, E.D. Zanotto, A.C.M. Rodrigues, M. Reza Dousti, A.S.S. de Camargo, C.J. Magon, I.D.A.A. Silva, Crystallization, mechanical, and optical properties of transparent, nanocrystalline gahnite glass-ceramics, *J. Am. Ceram. Soc.* 100 (2017) 1963–1975.
- [42] P. Shi, F. Wang, J. Zhu, B. Zhang, T. Zhao, Y. Wang, Y. Qin, Study on the Five dynasty sky-green glaze from Yaozhou kiln and its coloring mechanism, *Ceram. Int.* 43 (2017) 2943–2949.
- [43] J. Zhu, P. Shi, F. Wang, T. Zhao, Preparation of the moon-white glaze by carbothermic reduction of Fe₂O₃ and SiC, *J. Eur. Ceram. Soc.* 35 (2015) 4603–4609.
- [44] P. Shi, F. Wang, J. Zhu, H. Yang, Y. Wang, Y. Fang, B. Zhang, J. Wang, Amorphous photonic crystals and structural colors in the phase separation glaze, *J. Eur. Ceram. Soc.* 38 (2018) 2228–2233.
- [45] Y. Youn, J. Miller, K. Nwe, K.-J. Hwang, C. Choi, Y. Kim, S. Jin, Effects of metal dopings on CuCr₂O₄ pigment for use in concentrated solar power solar selective coatings, *ACS Appl. Energy Mater.* 2 (2019) 882–888.

CORRECTED PROOF